crystals

MDPI

Article

# Influence of Nonlocality on Transmittance and Reflectance of Hyperbolic Metamaterials

**Bartosz Janaszek [1,*], Marcin Kieliszczyk [1], Anna Tyszka-Zawadzka [1] and Paweł Szczepański [1,2]**

1 Institute of Microelectronics and Optoelectronics, Warsaw University of Technology, 75 Koszykowa Str., 00-662 Warsaw, Poland; m.kieliszczyk@imio.pw.edu.pl (M.K.); atyszka@elka.pw.edu.pl (A.T.-Z.); p.szczepanski@elka.pw.edu.pl (P.S.)
2 National Institute of Telecommunications, 1 Szachowa Str., 04-894 Warsaw, Poland
* Correspondence: b.janaszek@imio.pw.edu.pl

Received: 5 June 2020; Accepted: 2 July 2020; Published: 4 July 2020

check for updates

**Abstract:** In this paper we investigate transmittance and reflectance spectra of multilayer hyperbolic metamaterials in the presence of strong spatial dispersion. Our analysis revealed a number of intriguing optical phenomena, which cannot be predicted with the local response approximation, such as total reflectance for small angles of incidence or multiple transmittance peaks of resonant character (instead of the respective local counterparts, where almost complete transparency is predicted for small angles of incidence and the broad-angle transparency can be observed within a range of larger angles of incidence). We believe that the observed effects may serve as a working principle in a number of new potential applications, such as spatial filtering, biosensing, or beam steering.

**Keywords:** hyperbolic metamaterials; spatial dispersion; nonlocality; optical properties; spectral and spatial filtering

## 1. Introduction

Over the last two decades, a great deal of attention has been devoted to optical metamaterials providing new means for controlling wave propagation which are not achievable with conventional media [1–3]. A special class of uniaxially anisotropic metamaterials, called hyperbolic metamaterials (HMMs), have emerged as a particularly prospective media, due to their relatively high technological feasibility as well as wide applicability, including diffractionless lensing [4], biosensing [5–8], optical signal buffering/storing [9,10], efficient spectral [11], and spatial filtering [12], as well as many others [13–21].

The most common approach to predict the electromagnetic response of an HMM structure is the effective medium theory (EMT) which encompasses solely temporal dispersion, i.e., frequency-dependent effective electric permittivity tensor [13,22,23]. However, it has been shown that a correct description of realistic structures of finite dimensions often requires consideration of spatial dispersion, i.e., dependency of effective electric permittivity tensor components on wavevector [24–26]. Until now, a number of methods suitable for prediction of nonlocal response have been developed, including approaches based on Mie scattering theory [27] or Drude hydrodynamic model [28], as well as formalisms originating from the transfer matrix method [29,30].

The first studies devoted to spatial dispersion in hyperbolic media revealed that nonlocality substantially alters the intended performance of the structure by e.g., occurrence of an additional waveguide mode [31]. Further scientific efforts concerning nonlocality in HMMs were focused on investigating electromagnetic phenomena that are not present when spatial dispersion is negligible, such as direction controllable inverse transition radiation [32], spectral shift of intramolecular charge transfer emission [33], or the existence of Cherenkov radiation of controllable threshold [34]. Another branch of studies in this field was dedicated to possibility of controlling spatial dispersion at will. It has been shown that by proper layer arrangement in 1D HMM, e.g., Thue–Morse [35], or embedding nonuniform nanorods in 2D HMMs, e.g., cone-shaped [36], the nonlocality in HMMs can be greatly enhanced and employed, e.g., to obtain a stronger nonlinear response [36]. More recently, it has been also demonstrated that nonlocality can be efficiently controlled in spatially uniform hyperbolic metamaterials and may serve as a new mechanism for tailoring effective dispersion [37].

In this paper, we investigate the influence of nonlocality on reflectance and transmittance (RT) of an HMM structure. To unveil effects arising in the presence of strong spatial dispersion observed in an appropriately designed multilayer nanostructure [37], we perform numerical calculations based on a modified transfer matrix method (TMM), suitable for uniaxially and biaxially anisotropic media, for an HMM structure described with local and nonlocal EMT, respectively. By example of a multilayer structure based on graphene and silicon nitride, we investigate optical effects which arise in the presence of strong nonlocality, with a special emphasis on sensitivity of transmittance and reflectance to the angle of incidence. It is worth to underline that, since we do not consider spatial dispersion of constituent materials, all the observed nonlocal effects arise from appropriately chosen dimensions of the unit cell (in this case, thicknesses of the respective layers) [37]. Our analysis reveals a number of interesting nonlocality-induced effects, such as total reflectance for small angles of incidence or multiple transmittance peaks of resonant character (instead of the respective local counterparts, where almost complete transparency is predicted for small angles of incidence and the broad-angle transparency can be observed within a range of larger angles of incidence). We believe that controlling spatial dispersion in HMM structures opens new venues in various applications, e.g., requiring highly sensitive response to the angle of incidence.

## 2. Theoretical Model

In this section, we present theoretical background for our analysis. Firstly, we shortly discuss numerical models of the employed materials. Then, we present the local and nonlocal EMT formalisms, which are later used to describe the HMM structure. In the last subsection, we demonstrate a modified transfer matrix method (TMM), suitable for modelling propagation in planar biaxially anisotropic media, which is necessary when spatial dispersion is to be considered.

### 2.1. Dielectric Functions of Constituent Materials

We have selected graphene and silicon nitride (SiN) as nonmagnetic materials (relative magnetic permeability $\mu_{\mathrm{r}} = 1$) constituting the HMM structure, see Figure 1a. Complex relative electric permittivity of graphene is calculated based on the well-known Kubo formula [38], while the dielectric function of SiN is modelled based on the data available in the literature [39], which, within the considered spectral range, can be approximated with the help of Sellmeier formula [39], see Figure 1b.

It is worth to underline that of graphene and SiN are considered only in terms of their local response and have been chosen only as an example, which helps to demonstrate more general effects arising from the effective nonlocality in an appropriately designed periodic multilayer structure [37]. Technological feasibility of such structures is not impaired with significant difficulties and similar multilayer stacks have already been successfully manufactured [40,41]. Moreover, the chosen materials can be fabricated by means of well-established chemical vapor deposition [42,43] or reactive magnetron sputtering techniques [44,45].

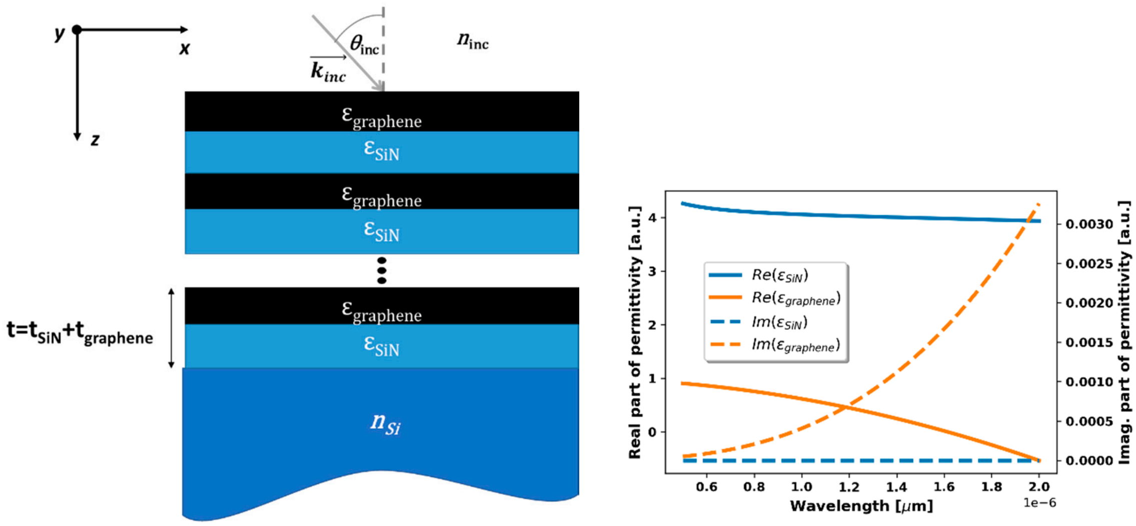


(a) (b)

**Figure 1.** Scheme of the considered multilayer structure (**a**) and complex electric permittivities of constituent materials (graphene and SiN) (**b**).

### 2.2. Effective Medium Theory

With the help of local effective medium theory, a structure consisting of periodically arranged isotropic subwavelength layers (see Figure 1a) can be described as a uniform uniaxially anisotropic medium with effective diagonal permittivity tensor $\overline{\overline{\varepsilon_{loc}}}(\omega) = diag\left(\ \varepsilon_{xx}^{loc},\ \ \varepsilon_{yy}^{loc},\ \ \varepsilon_{zz}^{loc}\ \right)$, with components of the following form [23]

$$\varepsilon_{xx}^{loc} = \varepsilon_{yy}^{loc} = \varepsilon_{\parallel}^{loc} = \tfrac{t_1\varepsilon_1(\omega)+t_2\varepsilon_2(\omega)}{t_1+t_2}, \quad \varepsilon_{zz}^{loc} = \frac{\varepsilon_1(\omega)\varepsilon_2(\omega)(t_1+t_2)}{t_1\varepsilon_2(\omega)+t_2\varepsilon_1(\omega)}, \tag{1}$$

where $\varepsilon_{\{1,2\}}$ and $t_{\{1,2\}}$ are relative electric permittivities and layer thicknesses of constituent materials. However, this approximation is not correct when spatial dispersion becomes substantial, e.g., when condition $t/\lambda \to 0$ is not fulfilled, where $t = t_1 + t_2$ is the dimension of the structure's unit cell (which, in this case, is the characteristic dimension of the structure) [46]. Thus, to predict the influence of nonlocality on the optical properties of an HMM structure, we need to employ a more comprehensive method, which allows for anticipating the impact of the wavevector on permittivity tensor components, apart from their frequency-dependent behavior.

In our analysis we use the formalism proposed by Chern [30], in which a two-constituent multilayer structure (see Figure 1a) can be effectively described as a biaxial anisotropic medium $\overline{\overline{\varepsilon}}(\omega, \vec{k}) = diag\left(\ \varepsilon_{xx}^{nloc},\ \ \varepsilon_{yy}^{nloc},\ \ \varepsilon_{zz}^{nloc}\ \right)$ having permittivity tensor components of the following form:

$$\varepsilon_{xx}^{nloc} = \frac{\varepsilon_{\parallel}^{loc} - \frac{\alpha}{12}k_0^2t^2}{1 - \frac{1}{12}k_z^2t^2}, \tag{2a}$$

$$\varepsilon_{yy}^{nloc} = \varepsilon_{\parallel}^{loc}\left(1 + \frac{1}{6}k_x^2t^2\right) + \frac{t^2}{12k_0^2}\left(k_z^4 - k_x^4\right) - \frac{\alpha}{12}k_0^2t^2, \tag{2b}$$

$$\varepsilon_{zz}^{nloc} = \frac{\varepsilon_{zz}^{loc} - \frac{\alpha}{12}k_0^2t^2}{1 + \frac{\varepsilon_{zz}^{loc}}{\varepsilon_{\parallel}^{loc}}\left(\frac{\beta}{12}k_x^2t^2 - \frac{\gamma}{6}k_0^2t^2\right)}, \tag{2c}$$

where $k_x$, $k_z$ are components of the wavevector $\vec{k}$ and $k_y = 0$ (due to the fact, that *x*-*z* plane is the plane of incidence; see Figure 1a, and α, β, and γ are given as:

$$\alpha = \left[f_1^2\varepsilon_1(\omega) + \left(1 - f_1^2\right)\varepsilon_2(\omega)\right]\left[\left(1 - f_2^2\right)\varepsilon_1(\omega) + f_2^2\varepsilon_2(\omega)\right], \tag{3a}$$

$$\beta = \frac{1}{\varepsilon_1(\omega)\varepsilon_2(\omega)}[(1 - 2f_1f_2)\varepsilon_1(\omega) + 2f_1f_2\varepsilon_2(\omega)][2f_1f_2\varepsilon_1(\omega) + (1 - 2f_1f_2)\varepsilon_2(\omega)], \tag{3b}$$

$$\begin{aligned}\gamma = \tfrac{1}{\varepsilon_1(\omega)\varepsilon_2(\omega)}&[f_1^3f_2\varepsilon_1^3(\omega) + f_1\left(1 - 2f_1^2f_2 + f_2^3\right)\varepsilon_1^2(\omega)\varepsilon_2(\omega) \\ &+ f_2\left(1 - f_1f_2^2 + f_1^3\right)\varepsilon_1(\omega)\varepsilon_2^2(\omega) + f_1f_2^3\varepsilon_2^3(\omega)],\end{aligned} \tag{3c}$$

and

$$f_i = t_i/t \tag{4}$$

is the so-called filling factor, where $i \in \{1,\ 2\}$. It is worth to underline that such nonlocal EMT formalism is suitable for correct description of multilayered nanostructures consisted of at least 2 unit cells [24].

The introduced EMT formalisms will be further employed to provide local and nonlocal electric permittivity tensors, which are required to calculate transmittance and reflectance by means of the transfer matrix method (as discussed in the next section).

### *2.3. Transfer Matrix Method*

In the principal coordinate system, permittivity tensor of a biaxial optical medium is of the diagonal form, i.e., $\overline{\overline{\varepsilon}} = diag\left(\ \varepsilon_x,\ \ \varepsilon_y,\ \ \varepsilon_z\ \right)$. In such a medium, two plane waves of orthogonal polarizations may exist, i.e., a transverse electric (TE) wave with field components $E_y$ and $H_x$, and a transverse magnetic (TM) wave with field components $H_y$ and $E_x$. In our case, we assume that time dependence of the waves is *exp(-jωt)* and the considered structure is nonuniform only in the *z* direction; thus, we have $\frac{\partial}{\partial x} = jk_x$, $\frac{\partial}{\partial y} = jk_y$ . Because the plane of incidence is in the *x*-*z* plane, $\frac{\partial}{\partial y} = jk_y = 0$. According to [47], starting from Maxwell equations, we may relate the field components $E_y$, $H_x$, $H_y$, and $E_x$ as follows:

$$\frac{\partial E_x}{\partial z'} = \left(\mu_r - \frac{\overline{k_x}^2}{\varepsilon_z}\right)\overline{H_y}, \tag{5a}$$

$$\frac{\partial E_y}{\partial z'} = \mu_r\overline{H_x}, \tag{5b}$$

$$\frac{\partial \overline{H_x}}{\partial z'} = \left(\varepsilon_y - \frac{\overline{k_x}^2}{\mu_r}\right)E_y, \tag{5c}$$

$$\frac{\partial \overline{H_y}}{\partial z'} = \varepsilon_x E_x, \tag{5d}$$

where $\vec{\overline{H}} = -j\sqrt{\frac{\mu_0}{\varepsilon_0}}\vec{H}$, $k_0 = \omega\sqrt{\varepsilon_0\mu_0}$, $z' = k_0 z$, $\overline{k_x} = \frac{k_x}{k_0}$ and $\mu_r$ denotes relative magnetic permeability (here, we consider nonmagnetic medium; thus, we have $\mu_r = 1$).

The Equations (5a–d) can be reformulated as a single matrix equation:

$$\frac{\partial\psi}{\partial z'} - \Omega\psi = 0, \tag{6}$$

where

$$\Omega = \begin{bmatrix} 0 & 0 & 0 & 1 - \frac{\overline{k_x}^2}{\varepsilon_z} \\ 0 & 0 & 1 & 0 \\ 0 & \varepsilon_y - \overline{k_x}^2 & 0 & 0 \\ -\varepsilon_x & 0 & 0 & 0 \end{bmatrix},\quad \psi = \begin{bmatrix} E_x(z') \\ E_y(z') \\ \overline{H_x}(z') \\ \overline{H_y}(z') \end{bmatrix}. \tag{7}$$

Solution to the Equation (7) can be written in the following form:

$$\psi(z') = e^{\Omega z'}\psi(0). \tag{8}$$

In order to solve this equation, we need to formulate an eigenvalue problem:

$$\psi(z') = We^{\lambda z'}c, \tag{9}$$

where $c = W^{-1}\psi(0)$ is a vector of field amplitudes, while $W$ and $\lambda$ are eigen-vector and eigen-value matrices of $\Omega$, respectively. Now, by employment of appropriate boundary conditions, i.e., $\psi_{in} = \psi_{layer}(0)$ and $\psi_{layer}(k_0L) = \psi_{out}$ (see Figure 2) and Equation (9), we can formulate a matrix equation describing the relationship between amplitudes in input ($c_{\text{in}}$) and output ($c_{\text{out}}$) media (see Figure 2):

$$c_{out} = W_{out}^{-1}W_{layer}e^{\lambda_{layer}k_0L}W_{layer}^{-1}W_{in} \cdot c_{in}, \tag{10}$$

where $L$ is the thickness of an anisotropic film, $c_{\{in,out\}} = \begin{bmatrix} c_{\{in,out\}}^{TE+} & c_{\{in,out\}}^{TE-} & c_{\{in,out\}}^{TM+} & c_{\{in,out\}}^{TM-} \end{bmatrix}$, while $W_{\{\text{in,out,layer}\}}$ are eigen-vector matrices of $\Omega_{\{\text{in,out,layer}\}}$ of the input/output medium and the anisotropic layer, respectively (see Figure 2). Thus, the transfer matrix for an anisotropic layer (see Figure 2) takes the following form

$$T = \begin{bmatrix} t_{11} & t_{12} & t_{13} & t_{14} \\ t_{21} & t_{22} & t_{23} & t_{24} \\ t_{31} & t_{32} & t_{33} & t_{34} \\ t_{41} & t_{42} & t_{43} & t_{44} \end{bmatrix} = W_{out}^{-1}W_{layer}e^{\lambda_{layer}k_0L}W_{layer}W_{in}. \tag{11}$$

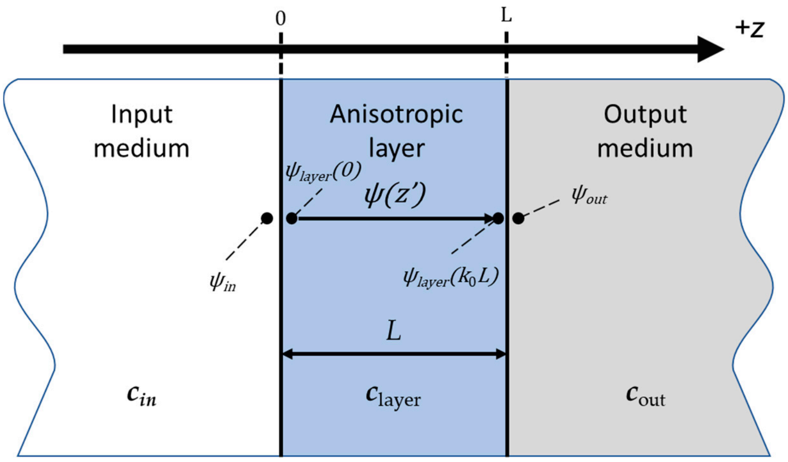


**Figure 2.** Schematic of transfer matrix formalism in a single layer system.

Thus, the reflectance coefficients for TE and TM polarization can be straightforwardly derived from matrix multiplication [48]:

$$\begin{bmatrix} c_{in}^{TE+} \\ c_{in}^{TE-} \\ c_{in}^{TM+} \\ c_{in}^{TM-} \end{bmatrix} = \begin{bmatrix} t_{11} & t_{12} & t_{13} & t_{14} \\ t_{21} & t_{22} & t_{23} & t_{24} \\ t_{31} & t_{32} & t_{33} & t_{34} \\ t_{41} & t_{42} & t_{43} & t_{44} \end{bmatrix}^{-1} \cdot \begin{bmatrix} c_{out}^{TE+} \\ 0 \\ c_{out}^{TM+} \\ 0 \end{bmatrix}, \tag{12}$$

resulting in:

$$R_{TE} \underset{c_{in}^{TM+}=0}{=} \left|\frac{c_{in}^{TE-}}{c_{in}^{TE+}}\right|^2 = \left|\frac{t_{21}t_{33} - t_{23}t_{31}}{t_{11}t_{33} - t_{13}t_{31}}\right|^2 \tag{13}$$

and

$$R_{TM} \underset{c_{in}^{TE+}=0}{=} \left|\frac{c_{in}^{TM-}}{c_{in}^{TM+}}\right|^2 = \left|\frac{t_{21}t_{43} - t_{41}t_{13}}{t_{11}t_{33} - t_{13}t_{31}}\right|^2. \tag{14}$$

Having noted that the losses of the considered materials are low (see Figure 1b), we can estimate transmittance of the anisotropic film as follows:

$$T_{TE} \approx 1 - R_{TE}, \tag{15}$$

$$T_{TM} \approx 1 - R_{TM}. \tag{16}$$

The Equations (13)–(16) will be further employed for the analysis of RT characteristics of the HMM structure depicted in the Figure 1a.

## 3. Results and Discussion

Here, we employed local and nonlocal EMT approaches to investigate influence of spatial dispersion on optical parameters of a hyperbolic metamaterial composed of periodically arranged layers of silicon nitride (SiN) and graphene, i.e., $\varepsilon_1 = \varepsilon_{\text{SiN}}(\omega)$ and $\varepsilon_2 = \varepsilon_{\text{graphene}}(\omega)$ (see Figure 1a). It is worth to reiterate that the obtained nonlocal response did not originate from the properties of constituent materials, but is a consequence of an appropriately designed multilayer arrangement, which led to a strong violation of the locality condition, i.e., $t/\lambda \to 0$ [37]. In this case, to observe a strong nonlocal response (according to [37]), we chose sufficiently thick layers constituting the unit cell, i.e., $t_1 = t_{\text{SiN}} = 150$ nm and $t_2 = t_{\text{graphene}} = 0.35$ nm (thickness of a graphene monolayer [49]). The total thickness of the HMM structure was set as $t_{\text{total}} = 1.5$ µm, which corresponds to 10 graphene/SiN bilayers—a number of unit cells ensuring validity of the EMT approach [20,40]. To determine the effects arising in the presence of nonlocality, the local and nonlocal permittivity tensor components of the considered HMM structure as well as respective RT characteristics plotted vs. wavelength were collated in the Figure 3a–d.

In general, effective permittivity tensor components obtained with local and nonlocal EMT become convergent for sufficiently long wavelengths (since $t/\lambda \to 0$) [37]. In the case discussed, due to strong nonlocal response provided by the proper design of the unit cell, the convergence within the considered spectral range occurs only for the permittivity tensor components $\varepsilon_{\parallel}^{loc}$ and $\varepsilon_{xx}^{nloc}$, $\varepsilon_{yy}^{nloc}$ ($\varepsilon_{xx}^{nloc} \to \varepsilon_{\parallel}^{loc}$ and $\varepsilon_{yy}^{nloc} \to \varepsilon_{\parallel}^{loc}$) (see Figure 3a,b). However, the local and nonlocal permittivity tensor components $\varepsilon_{zz}^{loc}$ and $\varepsilon_{zz}^{nloc}$ still differ considerably, causing inconsistency between respective RT characteristics over the wide spectral range (see Figure 3c,d). A particularly substantial difference can be observed within the range of shorter wavelengths ($\lambda < 1$µm), where a polarization-dependent RT as well as a total reflection, i.e., $R \approx 1$, occur, when nonlocality is considered. Since the nonlocal EMT inexplicitly considers plasmonic resonances, this effect may be related to the coupling between SPPs propagating at adjacent graphene/SiN interfaces [37,50,51].

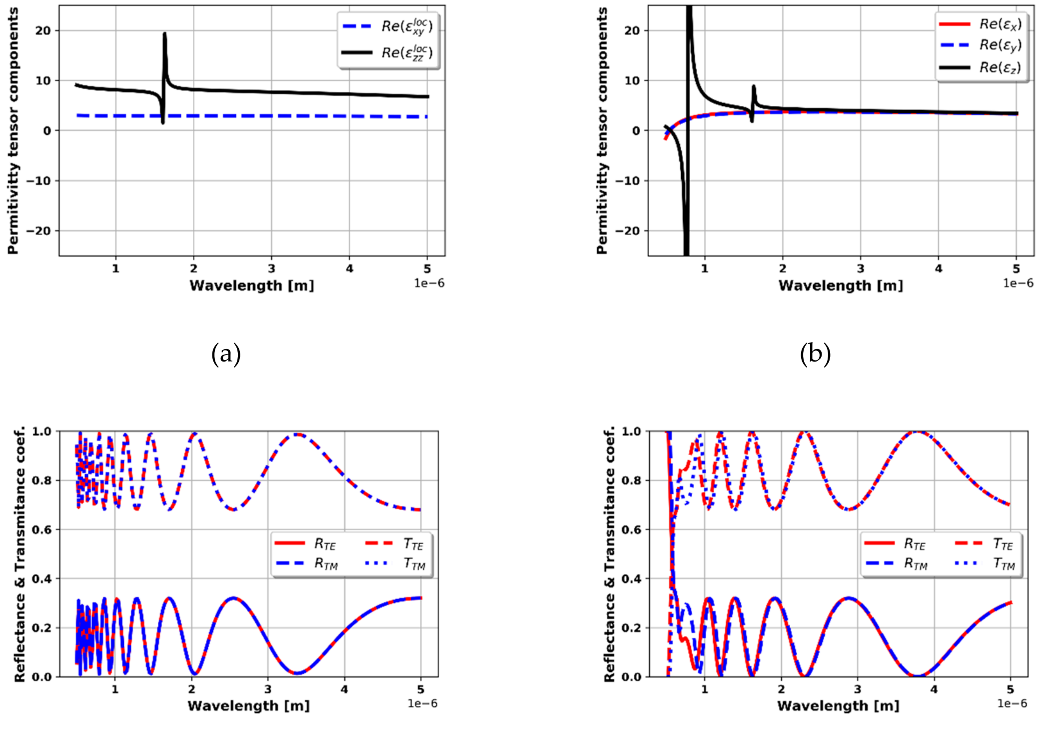


(a) (b) (c) (d)

**Figure 3.** Effective permittivity tensor components (**a**,**b**) and RT characteristics (**c**,**d**) plotted against wavelength for a structure described with local (**a**,**c**) and nonlocal EMT (**b**,**d**), respectively. The angle of incidence is fixed at 0°.

For shorter wavelengths ($\lambda < 1$ µm), the influence of nonlocality on RT is more evident; thus, we focused our further analysis on this spectral range. For this purpose, reflectance and transmittance (RT) coefficients within $\lambda$ = 0.5–0.7 µm and different angles of incidence, i.e., $\theta_{\text{inc}}$= 0° (Figure 4a–d), $\theta_{\text{inc}}$ = 45° (Figure 4e–g), $\theta_{\text{inc}}$ = 85° (Figure 4h–l) were calculated for a HMM structure described with local (Figure 4a,c,e,g–i,k) and nonlocal EMT model (Figure 4b,d,f,h,j,l).

Reflectance and transmittance spectra predicted with the help of nonlocal EMT substantially differed from the respective characteristics determined with the local approach, see Figure 4a–l. It can be observed that, in contrast to local approach, nonlocal response, even for normal incidence, was polarization-dependent and highly dispersive, i.e., small changes of wavelength caused a significant modification of both reflectance and transmittance (see Figure 4a–d). What is more, the presence of nonlocality led to the occurrence of a rejection band, i.e., the spectral range where $R \approx 1$ (see Figure 4a–f). It is also noteworthy that, in comparison to local RT, changing the angle incidence led to a much stronger alteration of nonlocal RT, which was caused by dependency of nonlocal permittivity tensor components on arrangement of wavevector of the incident radiation (see Equation (2a–c)). Thus, a responsible design should incorporate nonlocality to correctly predict spatial and spectral behavior of a multilayer HMM structure.

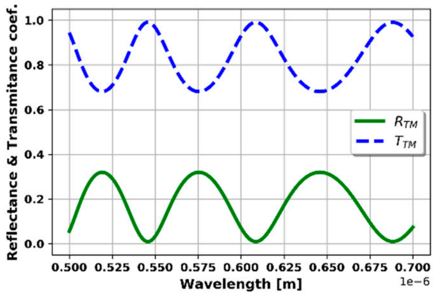


(a)

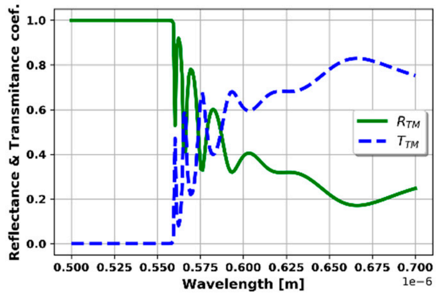


(b)

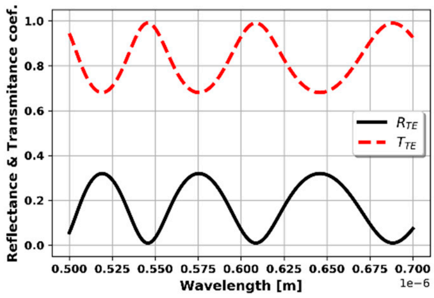


(c)

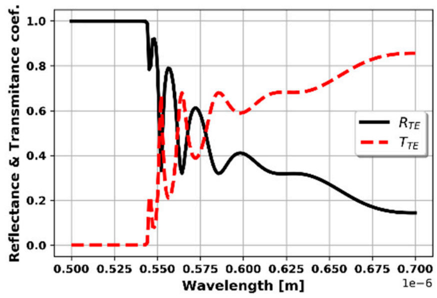


(d)

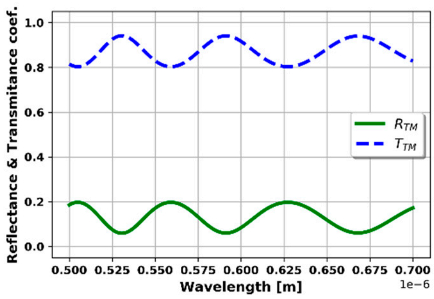


(e)

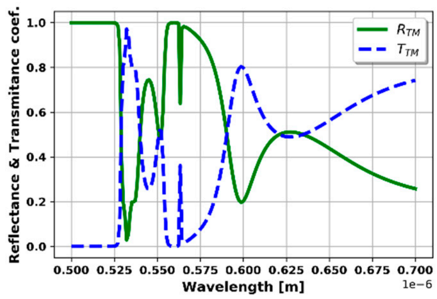


(f)

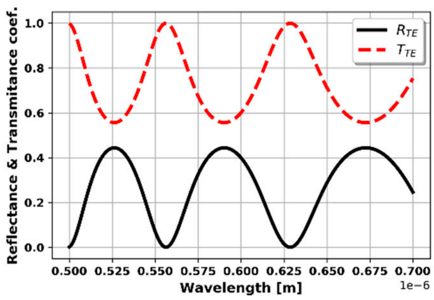


(g)

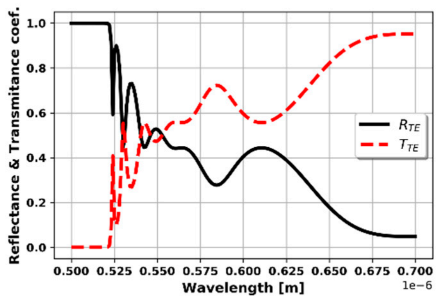


(h)

**Figure 4.** *Cont.*

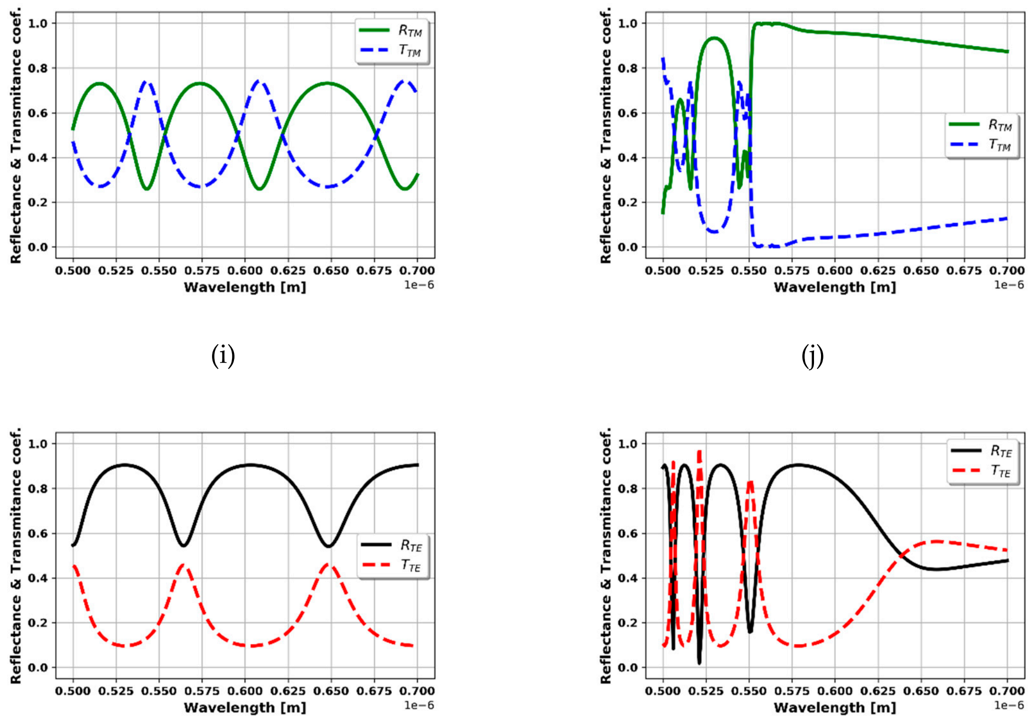


(i) (j)

(k) (l)

**Figure 4.** Transmittance and reflectance spectra for a structure described by local (**a**,**c**,**e**,**g**,**i**,**k**) an nonlocal EMT (**b**,**d**,**f**,**h**,**j**,**l**) for various angles of incidence: 0° (**a**–**d**), 45° (**c**–**f**), and 85° (**e**–**l**).

Let us now consider influence of the angle of incidence on optical properties of the considered structure. For this aim, permittivity tensor components along with transmittance and reflectance of the structure described with local (Figure 5a,c,e) and nonlocal EMT (Figure 5b,d,f) were plotted versus angle of incidence at a fixed wavelength of $\lambda_0 = 0.55$ µm. For the purpose of analysis, we considered free space ($n_{\mathrm{in}} = 1$) as the incident medium.

The properties of the structure observed in the angular domain were still substantially influenced by the presence of nonlocality, compare Figure 5a,c,e and Figure 5b,d,f. It can be observed that, within the range of small angles, the structure reveals complete reflection for TM polarization, i.e., $R \approx 1$, which was drastically different from the response predicted with the help of local approach, i.e., almost complete transparency $T \approx 1$, compare Figure 5c,e and Figure 5d,f. What is more, the nonlocal reflectance and transmittance for TE polarization were also significantly different from the respective local characteristics. Furthermore, for larger angles of incidence, instead of a single broad minimum of reflectance predicted with the local approach, we obtained multiple minima of narrow width for both light polarizations, which may be useful in terms of potential applications, e.g., highly sensitive spatial filter.

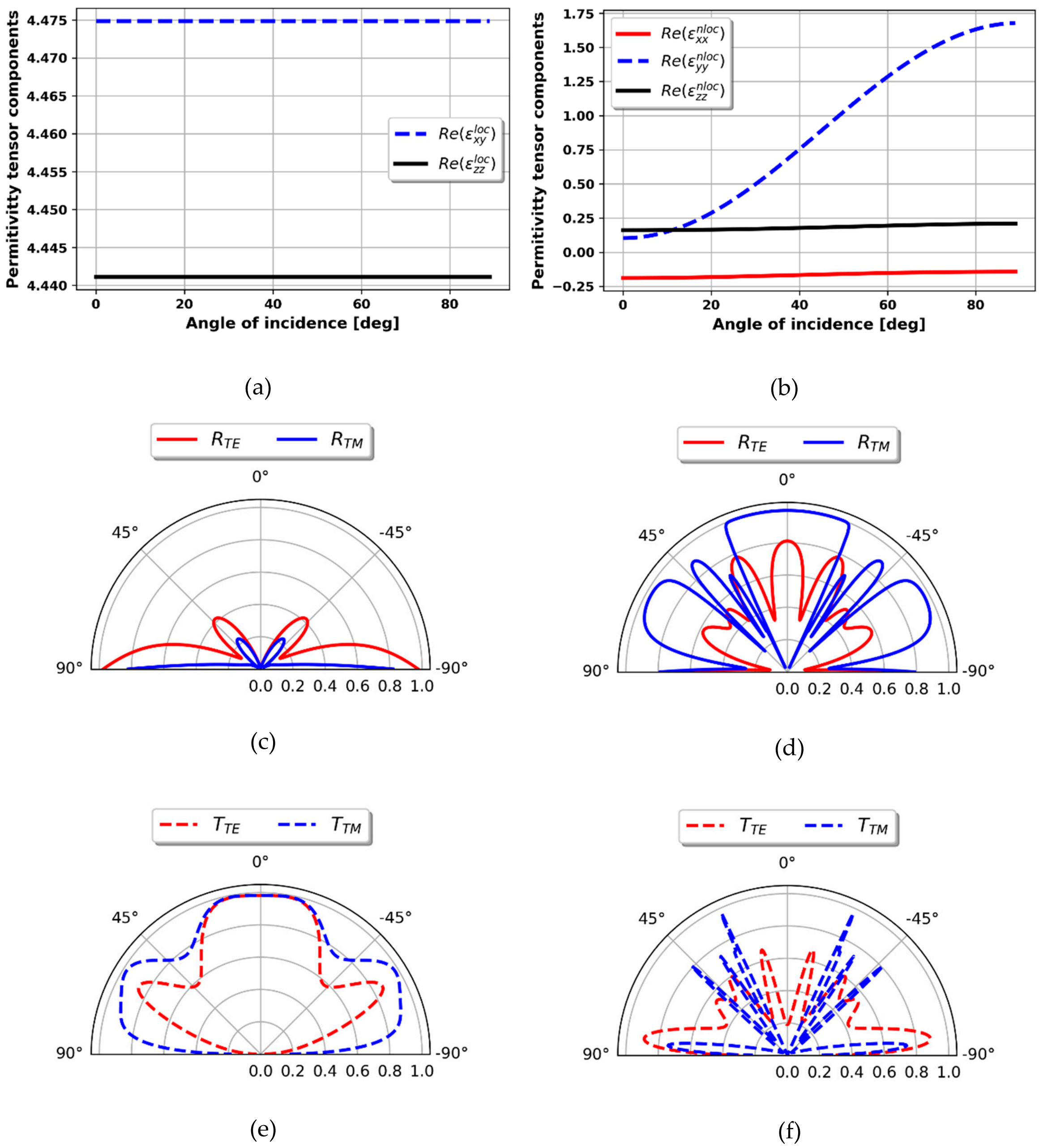


**Figure 5.** Effective permittivity tensor components (**a**,**b**), reflectivity (**c**,**d**), and transmittance (**e**,**f**) illustrated as a function of angle of incidence for a structure described with local (**a**,**c**,**e**) and nonlocal EMT (**b**,**d**,**f**). The wavelength is fixed at 0.55 µm.

To fully explore the influence of spatial dispersion, we calculated local and nonlocal transmittance as a function of angle of incidence for incident media characterized with various refractive indices $n_{\text{in}} = 1.5$ (Figure 6a,b), 2 (Figure 6c,d), and 3 (Figure 6e,f). The influence of nonlocality was particularly significant for TM polarization, for which we can observe multiple narrow peaks of transmittance that cannot be predicted with local EMT approach, compare Figure 6a,c,e and Figure 6b,d,f. On the other hand, we can observe an opposite effect for nonlocal TE polarization transmittance, for which the angular sensitivity was diminished with respect to its local counterpart, i.e., nonlocal transmittance is less sensitive to the angle of incidence.

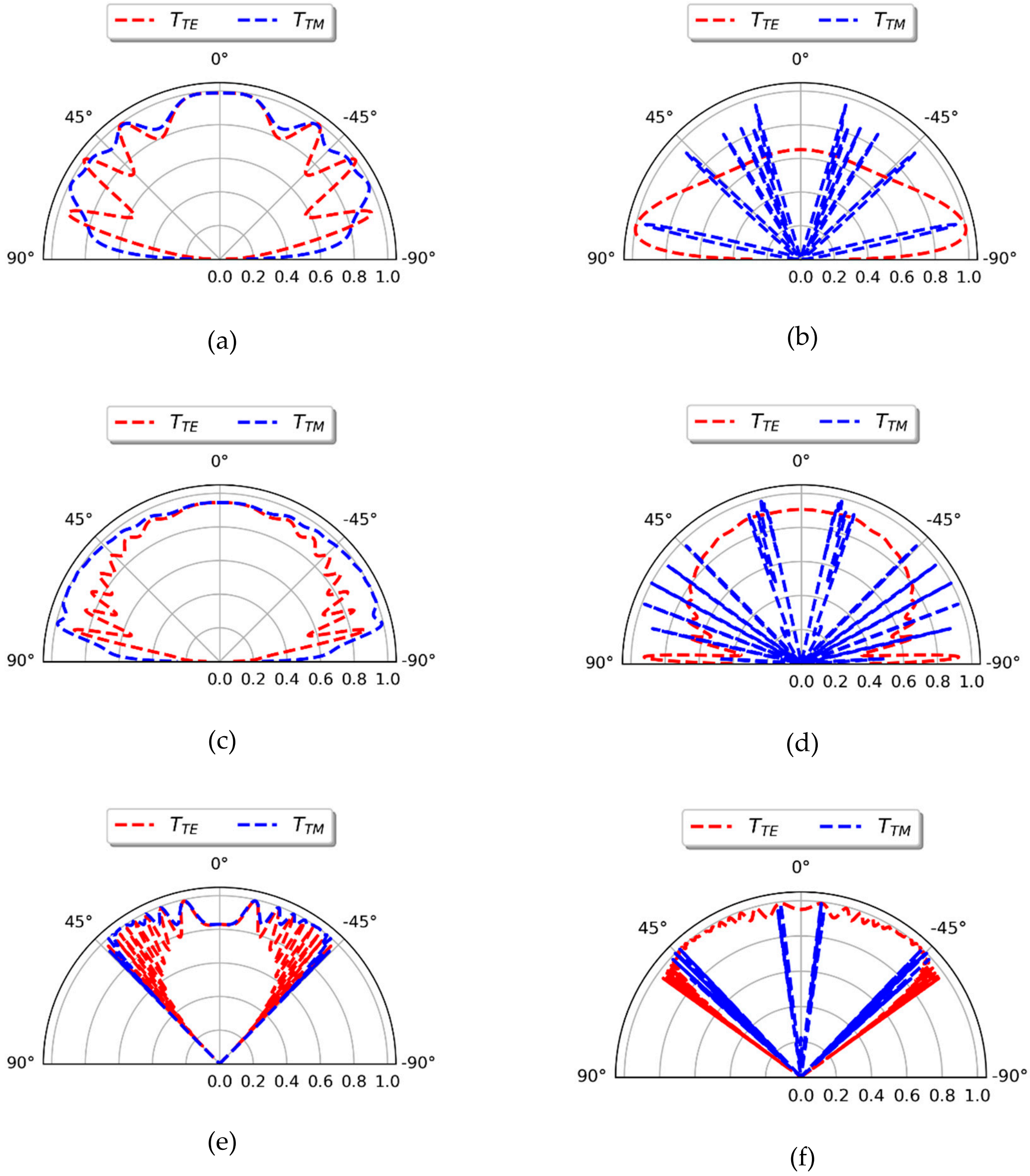


**Figure 6.** Transmittance illustrated as a function of angle of incidence for the structure described with local (**a**,**c**,**e**) and nonlocal EMT (**b**,**d**,**f**) for various refractive indices of the incident medium $n_{\mathrm{in}} = 1.5$ (**a**,**b**), 2 (**c**,**d**), and 3 (**e**,**f**). The wavelength is fixed at 0.55 µm.

In general, increasing the refractive index of the incident medium substantially alters transmittance of an arbitrary optical system. However, in our case, a clear-cut tendency in alteration of nonlocal transmittance cannot be observed, since the change of the refractive index, and thus the magnitude of the incident wavevector, modifies nonlocal permittivity tensor components of the medium (see Equation (2a–c)). Additionally, due to different material properties perceived by the incident wave, we can also observe a wider acceptance cone, i.e., higher value of the critical angle for total internal refraction, compare Figure 6e,f. It is worth noting that nonlocal transmittance of TM polarization preserves a discrete character, i.e., multiple narrow peaks, for an arbitrary medium, which may serve as a mechanism for experimental verification of the presence of nonlocality. Thus, the consideration of nonlocal effects allows us not only to predict a possible deviation from the intended performance, but also to exploit additional effects arising from nonlocality for the purpose of new potential applications requiring, e.g., highly efficient spatial discrimination. We believe that the nonlocality in HMMs can be viewed as an advantage and may help to deploy new exciting applications requiring tailored spatial and spectral response.

## 4. Conclusions

Within this paper, we have investigated local and nonlocal optical response of an HMM structure. By example of a multilayer structure based on graphene and SiN, represented by respective local dielectric functions, we demonstrated a substantial difference between local and nonlocal response by revealing effects arising in the presence of strong spatial dispersion arising in an appropriately designed HMM structure, such as a rejection band within the range of shorter wavelengths or highly selective angular transmittance characteristics. We believe that these distinctive features of nonlocal response that cannot be predicted with the help of local approximation, may serve as a working principle for a number of new potential applications, such as spatial filtering, biosensing, or beam steering.

**Author Contributions:** Conceptualization, P.S. and B.J.; methodology, P.S., M.K., and B.J.; software, M.K. and B.J.; formal analysis, A.T.-Z.; investigation, B.J.; writing—original draft preparation, M.K. and B.J.; writing—review and editing, P.S.; and visualization, B.J. All authors have read and agreed to the published version of the manuscript.

**Funding:** This research was funded by the National Science Centre (Poland, grant number UMO-2016/23/N/ST7/03573) and the National Centre for Research and Development (Poland, grant number TECHMATSTRATEG1/347012/3/NCBR/2017).

**Conflicts of Interest:** The authors declare no conflict of interest. The funders had no role in the design of the study; in the collection, analyses, or interpretation of data; in the writing of the manuscript, or in the decision to publish the results.

## References

1. Shalaev, V.M. Optical negative-index metamaterials. *Nat. Photonics.* **2007**, *1*, 41–48. [CrossRef]
2. Cummer, S.A.; Christensen, J.; Alù, A. Controlling sound with acoustic metamaterials. *Nat. Rev. Mater.* **2016**, *1*, 16001. [CrossRef]
3. Zhu, S.; Zhang, X. Metamaterials: Artificial materials beyond nature. *Natl. Sci. Rev.* **2018**, *5*, 131. [CrossRef]
4. Sun, J.; Litchinitser, N.M. Toward Practical, Subwavelength, Visible-Light Photolithography with Hyperlens. *ACS Nano* **2018**, *12*, 542–548. [CrossRef] [PubMed]
5. Sreekanth, K.V.; Alapan, Y.; ElKabbash, M.; Ilker, E.; Hinczewski, M.; Gurkan, U.A.; De Luca, A.; Strangi, G. Extreme sensitivity biosensing platform based on hyperbolic metamaterials. *Nat. Mater.* **2016**, *15*, 621–627. [CrossRef]
6. Baqir, M.A.; Farmani, A.; Fatima, T.; Raza, M.R.; Shaukat, S.F.; Mir, A. Nanoscale, tunable, and highly sensitive biosensor utilizing hyperbolic metamaterials in the near-infrared range. *Appl. Opt.* **2018**, *57*, 9447. [CrossRef]
7. Kabashin, A.; Evans, P.; Pastkovsky, S.; Wurtz, G.A.; Hendren, W.; Atkinson, R.; Pollard, R.; Podolskiy, V.A.; Zayats, A.V. Plasmonic nanorod metamaterials for biosensing. *Nat. Mater.* **2009**, *8*, 867–871. [CrossRef]
8. Shkondin, E.; Repän, T.; Esmail Aryaee Panah, M.; Lavrinenko, A.V.; Takayama, O. High aspect ratio plasmonic nanotrench structures with large active surface area for label-free mid-infrared molecular absorption sensing. *ACS Appl. Nano Mater.* **2018**, *1*, 1212–1218. [CrossRef]
9. Neira, A.D.; Wurtz, G.A.; Zayats, A.V. Superluminal and stopped light due to mode coupling in confined hyperbolic metamaterial waveguides. *Sci. Rep.* **2015**, *5*, 17678. [CrossRef]
10. Tyszka-Zawadzka, A.; Janaszek, B.; Szczepański, P. Tunable slow light in graphene-based hyperbolic metamaterial waveguide operating in SCLU telecom bands. *Opt. Express* **2017**, *25*, 7263. [CrossRef]
11. Kieliszczyk, M.; Janaszek, B.; Tyszka-Zawadzka, A.; Szczepański, P. Tunable spectral and spatial filters for the mid-infrared based on hyperbolic metamaterials. *Appl. Opt.* **2018**, *57*, 1182–1187. [CrossRef]
12. Ghoshroy, A.; Adams, W.; Zhang, X.; Güney, D.Ö. Hyperbolic metamaterial as a tunable near-field spatial filter to implement active plasmon-injection loss compensation. *Phys. Rev. Appl.* **2018**, *10*, 024018. [CrossRef]
13. Lu, D.; Qian, H.; Wang, K.; Shen, H.; Wei, F.; Jiang, Y.; Fullerton, E.E.; Yu, P.K.L.; Liu, Z. Nanostructuring Multilayer Hyperbolic Metamaterials for Ultrafast and Bright Green InGaN Quantum Wells. *Adv. Mater.* **2018**, *30*, 1706411. [CrossRef] [PubMed]

14. Barbillon, G.; Sakat, E.; Hugonin, J.-P.; Biehs, S.-A.; Ben-Abdallah, P. True thermal antenna with hyperbolic metamaterials. *Opt. Express.* **2017**, *25*, 23356. [CrossRef] [PubMed]
15. Huo, P.; Zhang, S.; Liang, Y.; Lu, Y.; Xu, T. Hyperbolic Metamaterials and Metasurfaces: Fundamentals and Applications. *Adv. Opt. Mater.* **2019**, *7*, 1801616. [CrossRef]
16. Pianelli, A.; Kowerdziej, R.; Dudek, M.; Sielezin, K.; Olifierczuk, M.; Parka, J. Graphene-based hyperbolic metamaterial as a switchable reflection modulator. *Opt. Express* **2020**, *28*, 6708. [CrossRef]
17. Poddubny, A.; Iorsh, I.; Belov, P.; Kivshar, Y. Hyperbolic metamaterials. *Nat. Photon.* **2013**, *7*, 948–957. [CrossRef]
18. Shekhar, P.; Atkinson, J.; Jacob, Z. Hyperbolic metamaterials: Fundamentals and applications. *Nano Converg.* **2014**, *1*, 14. [CrossRef]
19. Ferrari, L.; Wu, C.; Lepage, D.; Zhang, X.; Liu, Z. Hyperbolic metamaterials and their applications. *Prog. Quantum Electron.* **2015**, *40*, 1–40. [CrossRef]
20. Takayama, O.; Lavrinenko, A.V. Optics with hyperbolic materials. *JOSA B* **2019**, *36*, F38–F48. [CrossRef]
21. Guo, Z.; Jiang, H.; Chen, H. Hyperbolic metamaterials: From dispersion manipulation to applications. *J. Appl. Phys.* **2020**, *127*, 071101. [CrossRef]
22. Campione, S.; Klem, J.F.; Liu, S.; Montano, I.; Sinclair, M.B.; Luk, T.S. Experimental Evidence of the Lorentz-Like Effective Medium Resonance in Semiconductor Hyperbolic Metamaterials Using Strong Coupling to Plasmonic Metasurfaces. *IEEE Trans. Antennas Propag.* **2020**, *68*, 1748–1754. [CrossRef]
23. Janaszek, B.; Kieliszczyk, M.; Tyszka-Zawadzka, A.; Szczepański, P. Multiresonance response in hyperbolic metamaterials. *Appl. Opt.* **2018**, *57*, 2135. [CrossRef]
24. Elser, J.; Podolskiy, V.A.; Salakhutdinov, I.; Avrutsky, I. Nonlocal effects in effective-medium response of nanolayered metamaterials. *Appl. Phys. Lett.* **2007**, *90*, 191109. [CrossRef]
25. Correas-Serrano, D.; Gomez-Diaz, J.S.; Tymchenko, M.; Alù, A. Nonlocal response of hyperbolic metasurfaces. *Opt. Express* **2015**, *23*, 29434. [CrossRef] [PubMed]
26. Shalin, A.S.; Ginzburg, P.; Orlov, A.A.; Iorsh, I.; Belov, P.A.; Kivshar, Y.S.; Zayats, A.V. Scattering suppression from arbitrary objects in spatially dispersive layered metamaterials. *Phys. Rev. B* **2015**, *91*, 125426. [CrossRef]
27. Geng, T.; Zhuang, S.; Gao, J.; Yang, X. Nonlocal effective medium approximation for metallic nanorod metamaterials. *Phys. Rev. B* **2015**, *91*, 245128. [CrossRef]
28. Yan, W.; Asger Mortensen, N.; Wubs, M. Hyperbolic metamaterial lens with hydrodynamic nonlocal response. *Opt. Express* **2013**, *21*, 15026. [CrossRef]
29. Chebykin, A.V.; Orlov, A.A.; Simovski, C.R.; Kivshar, Y.S.; Belov, P.A. Nonlocal effective parameters of multilayered metal-dielectric metamaterials. *Phys. Rev. B* **2012**, *86*, 115420. [CrossRef]
30. Chern, R.-L. Spatial dispersion and nonlocal effective permittivity for periodic layered metamaterials. *Opt. Express* **2013**, *21*, 16514. [CrossRef]
31. Pollard, R.J.; Murphy, A.; Hendren, W.R.; Evans, P.R.; Atkinson, R.; Wurtz, G.A.; Zayats, A.V.; Podolskiy, V.A. Optical Nonlocalities and Additional Waves in Epsilon-Near-Zero Metamaterials. *Phys. Rev. Lett.* **2009**, *102*, 127405. [CrossRef] [PubMed]
32. Gong, S.; Hu, M.; Wu, Z.; Pan, H.; Wang, H.; Zhang, K.; Zhong, R.; Zhou, J.; Zhao, T.; Liu, D.; et al. Direction controllable inverse transition radiation from the spatial dispersion in a graphene-dielectric stack. *Photonics Res.* **2019**, *7*, 1154. [CrossRef]
33. Lee, K.J.; Lee, Y.U.; Fages, F.; Ribierre, J.-C.; Wu, J.W.; D'Aléo, A. Blue-Shifting Intramolecular Charge Transfer Emission by Nonlocal Effect of Hyperbolic Metamaterials. *Nano Lett.* **2018**, *18*, 1476–1482. [CrossRef] [PubMed]
34. Hu, H.; Gao, D.; Lin, X.; Hou, S.; Zhang, B.; Wang, Q.J.; Luo, Y. Directing Cherenkov photons with spatial nonlocality. *Nanophotonics* **2020**, 20200135. [CrossRef]
35. Savoia, S.; Castaldi, G.; Galdi, V. Optical nonlocality in multilayered hyperbolic metamaterials based on Thue-Morse superlattices. *Phys. Rev. B* **2013**, *87*, 235116. [CrossRef]
36. Wells, B.; Kudyshev, Z.A.; Litchinitser, N.; Podolskiy, V.A. Nonlocal Effects in Transition Hyperbolic Metamaterials. *ACS Photonics* **2017**, *4*, 2470–2478. [CrossRef]
37. Janaszek, B.; Szczepański, P. Effect of nonlocality in spatially uniform anisotropic metamaterials. *Opt. Express* **2020**, *28*, 15447. [CrossRef]
38. Hanson, G.W. Dyadic Green's Functions for an Anisotropic, Non-Local Model of Biased Graphene. *IEEE Trans. Antennas Propag.* **2008**, *56*, 747–757. [CrossRef]

39. Luke, K.; Okawachi, Y.; Lamont, M.R.E.; Gaeta, A.L.; Lipson, M. Broadband mid-infrared frequency comb generation in a $Si_3N_4$ microresonator. *Opt. Lett.* **2015**, *40*, 4823. [CrossRef]
40. Chang, Y.-C.; Liu, C.-H.; Liu, C.-H.; Zhang, S.; Marder, S.R.; Narimanov, E.E.; Zhong, Z.; Norris, T.B. Realization of mid-infrared graphene hyperbolic metamaterials. *Nat. Commun.* **2016**, *7*, 10568. [CrossRef]
41. Mroczyński, R.; Iwanicki, D.; Fetliński, B.; Ożga, M.; Świniarski, M.; Gertych, A.; Zdrojek, M.; Godlewski, M. Optimization of Ultra-Thin Pulsed-DC Magnetron Sputtered Aluminum Films for the Technology of Hyperbolic Metamaterials. *Crystals* **2020**, *10*, 384. [CrossRef]
42. Muñoz, R.; Gómez-Aleixandre, C. Review of CVD Synthesis of Graphene: Review of CVD Synthesis of Graphene. *Chem. Vap. Depos.* **2013**, *19*, 297–322. [CrossRef]
43. Du, H. Oxidation Studies of Crystalline CVD Silicon Nitride. *J. Electrochem. Soc.* **1989**, *136*, 1527. [CrossRef]
44. Mroczyński, R.; Beck, R. Silicon Oxynitride Layers Fabricated by Plasma Enhanced Chemical Vapor Deposition (PECVD) for CMOS Devices. In *Proceedings of the ECS Transactions*; ECS: Vienna, Austria, 2009; pp. 797–804.
45. Mroczyński, R.; Szymańska, M.; Głuszewski, W. Reactive magnetron sputtered hafnium oxide layers for nonvolatile semiconductor memory devices. *J. Vac. Sci. Technol. B Nanotechnol. Microelectron. Mater. Process. Meas. Phenom.* **2015**, *33*, 01A113. [CrossRef]
46. Agranovich, V.M.; Ginzburg, V. Spatial Dispersion in Crystal Optics. In *Crystal Optics with Spatial Dispersion, and Excitons*, 2nd ed.; Springer-Verlag Berlin Heidelberg: New York, NY, USA, 1984; ISBN 978-3-662-02406-5.
47. Berreman, D.W. Optics in Stratified and Anisotropic Media: 4 × 4-Matrix Formulation. *J. Opt. Soc. Am.* **1972**, *62*, 502. [CrossRef]
48. Yeh, P. Optics of Anisotropic Layered Media. In *Optical Waves in Layered Media*, 1st ed.; Wiley: New York, NY, USA, 1988; ISBN 978-0-471-82866-2.
49. Janaszek, B.; Tyszka-Zawadzka, A.; Szczepański, P. Tunable graphene-based hyperbolic metamaterial operating in SCLU telecom bands. *Opt. Express* **2016**, *24*, 24129. [CrossRef]
50. Maier, S.A. Surface plasmon polaritons at metal/insulator interfaces. In *Plasmonics: Fundamentals and Applications*, 1st ed.; Springer: New York, NY, USA, 2007; ISBN 978-0387-33150-8.
51. Prade, B.; Vinet, J.Y.; Mysyrowicz, A. Guided optical waves in planar heterostructures with negative dielectric constant. *Phys. Rev. B* **1991**, *44*, 13556. [CrossRef]